machines

MDPI

Article

Thermal Behavior Improvement in Induction Motors Using a Pulse-Width Phase Shift Triangle Modulation Technique in Multilevel H-Bridge Inverters

Francisco M. Perez-Hidalgo [1], Juan-Ramón Heredia-Larrubia [2,*], Antonio Ruiz-Gonzalez [1] and Mario Meco-Gutierrez [1]

[1] Department of Electrical Engineering, University of Malaga, 29071 Malaga, Spain; fmperez@uma.es (F.M.P.-H.); afruiz@uma.es (A.R.-G.); mjmeco@uma.es (M.M.-G.)
[2] Department of Electronic Technology, University of Malaga, 29071 Malaga, Spain
* Correspondence: jrheredia@uma.es

Abstract

This study investigates the thermal performance of induction motors powered by multilevel H-bridge inverters using a novel pulse-width phase shift triangle modulation (PSTM-PWM) technique. Conventional PWM methods introduce significant harmonic distortion, increasing copper and iron losses and causing overheating and reduced motor lifespan. Through experimental testing and comparison with standard PWM techniques (LS-PWM and PS-PWM), the proposed PSTM-PWM reduces harmonic distortion by up to 64% compared to the worst one and internal motor losses by up to 5.5%. A first-order thermal model is used to predict motor temperature, validated with direct thermocouple measurements and infrared thermography. The results also indicate that the PSTM-PWM technique improves thermal performance, particularly at a triangular waveform peak value of 3.5 V, reducing temperature by around 6% and offering a practical and simple solution for industrial motor drive applications. The modulation order was set to M = 7 to reduce both the losses in the power inverter and to prevent the generation of very high voltage pulses (high dV/dt), which can deteriorate the insulation of the induction motor windings over time.

Keywords: induction motor heating; multilevel inverter; harmonic reduction; thermal modeling; PWM techniques; EN50160 compliance

Academic Editor: Mohamed Abdelrahem

Received: 17 June 2025
Revised: 31 July 2025
Accepted: 6 August 2025
Published: 8 August 2025

Citation: Perez-Hidalgo, F.M.; Heredia-Larrubia, J.-R.; Ruiz-Gonzalez, A.; Meco-Gutierrez, M. Thermal Behavior Improvement in Induction Motors Using a Pulse-Width Phase Shift Triangle Modulation Technique in Multilevel H-Bridge Inverters. *Machines* **2025**, *13*, 703. https://doi.org/10.3390/machines13080703

1. Introduction

Induction motors represent one of the most widely used elements in industrial and commercial electrical systems due to their robustness, efficiency, and low maintenance. In recent years, more than 53% of the world's electrical energy consumption has been used by electric motor systems, and more than 70% of this electrical energy is used by induction motors with low efficiencies [1].

However, the electrical environment in which these systems operate has changed significantly with the proliferation of nonlinear loads such as power converters, which introduce voltage and current harmonics into the power supply. This harmonic distortion, although often ignored under normal operating conditions, can have severe thermal effects on induction motors, compromising their lifespans, energy efficiency, and operational reliability [2].

Harmonics increase stator and rotor copper losses, as well as iron losses due to higher-than-fundamental frequency harmonics. These increased losses translate directly into

increased motor heating, which can exceed the thermal limits of the winding insulation, especially in critical areas such as winding heads. In addition, low-order harmonics (such as fifth and seventh harmonics) generate pulsating torques that further contribute to unwanted mechanical and thermal stresses [3,4].

The thermal impact of harmonics on induction motors is a complex and multifactorial phenomenon, as it depends on the frequency and magnitude of the harmonics, the type of load, the degree of ventilation, and the thermal insulation characteristics of the motor. Although international standards such as IEEE 519 and IEC 60034-17 recommend total harmonic distortion (THD) limits, these limits are exceeded in many industrial applications, resulting in operating conditions outside the rated design [5,6]. When these power inverters are used, these harmonics appear. Whenever possible, the lowest modulation index of the converter is desirable to reduce the switching losses of the power inverter and to avoid the generation of very high voltage pulses (high dV/dt), which can deteriorate the insulation of the motor windings over time [7,8].

The thermal effect can be explained by the following:

1. Increased losses due to Joule effect (copper losses)—Current harmonics have frequencies higher than the fundamental (50 or 60 Hz). As a consequence, the total copper losses increase. In addition, these harmonics circulate through both the stator and rotor (in the form of eddy currents), aggravating the Joule losses in both parts.
2. Additional losses in the iron (magnetic core)—The harmonic components of the voltage generate rapid variations in the magnetic flux in the motor core, increasing hysteresis losses, which depend on the frequency and magnetization cycle, and eddy current losses; these increase quadratically with frequency. Both mechanisms contribute to additional heat dissipation in the stator core and rotor [9].
3. Skin effect—At higher harmonic frequencies, the current tends to concentrate at the periphery of the conductor, reducing the effective cross-section through which the current flows. This increases the apparent resistance of the conductor and, therefore, the resistive losses. This phenomenon is more noticeable in large motors but also has an impact on small motors under high distortion [10].
4. Less effective ventilation due to pulsating torque—Some harmonics, especially those of low odd order (such as the fifth or seventh), produce pulsations in the electromagnetic torque that can cause vibrations, resonances, and unwanted changes in the speed of the motor fan (if coupled to the shaft). This reduces the efficiency of the motor's cooling system, further raising its temperature [11].
5. Localized thermal imbalance—The effect of harmonics is not uniform throughout the motor; certain areas, such as the turn heads or stator slots, can become hotter due to winding geometry and non-uniform loss distribution. This can accelerate insulation deterioration and lead to premature failure [12].

Induction motors are designed to operate within a specific temperature range, defined by the thermal insulation class of their windings. If this range is exceeded, adverse effects are generated that accelerate motor aging and can lead to total failure. The problems caused by overheating in induction motors are as follows:

a. Deterioration of the winding insulation—The high temperature degrades the dielectric material covering the stator conductors. It is estimated that for every 10 °C above the limit, the lifespan of the insulation is reduced by half (Montsinger's rule). This can lead to short circuits between turns or phases, resulting in catastrophic electrical failures [13–16].
b. Efficiency loss—At higher temperatures, copper resistance increases, which increases the I^2R losses. This reduces the energy efficiency of the motor and increases the electrical consumption [17].

c. Rotor damage—Although the rotor is more thermally robust, it also suffers from temperature increases. Mechanical deformation, uneven expansion, or weakening of the shaft may also occur [18].
d. Bearing and lubrication failures—Excessive heat can degrade lubricating grease, causing premature bearing wear. This leads to vibration, noise, and mechanical failure. This decreases the thermal performance of the housing [19].

The most critical part of an induction motor in terms of heating is the stator windings, especially the coil heads. These areas are prone to overheating due to the accumulation of thermal losses and less-efficient heat dissipation. Overheating in these areas can degrade insulation, which can lead to short circuits between turns and catastrophic motor failure.

In summary, an induction motor should not be heated beyond its thermal capacity because this shortens its life, affects its electrical and mechanical performance, and can lead to critical failures. Keeping the motor within its safe thermal range is essential to ensuring its reliability.

Power inverters are widely used to power induction motors because they can control the frequency and amplitude of applied voltage, allowing speed and torque to be adjusted efficiently. However, the switching operation of these inverters—especially in pulse-width modulation (PWM) topologies—inevitably introduces harmonic components into the voltage and current supplied to the motor.

Standard EN50160 [20] defines the characteristics of the voltage supplied by public electricity distribution networks, including limits on harmonic distortion. Although it is not specifically aimed at electric motors, it does establish power quality levels that directly affect their operation and durability. This standard serves as a reference to ensure compatibility between the grid and the equipment connected to it (such as motors). Poor wave quality can cause motors to fail to perform their function properly or suffer premature failure.

Unlike an ideal sinusoidal power supply, the output signal of an inverter is composed of a sequence of pulses that approximates a desired sine wave. This nonlinear waveform contains a series of high-frequency harmonics that propagate into the motor [21–23]. The voltage harmonics induce harmonic currents in the stator windings, resulting in the undesirable effects discussed earlier. In this context, multilevel inverters—such as diode-clamp (NPC) [24,25], flying capacitors (FCs) [26], and cascade H-bridge (CHB) inverters [27]—can reduce harmonic distortion, over-voltages, and switching losses, improving both system efficiency and motor life [28–30]. The goal of this research is to present a modulation technique for multilevel H-bridge inverters that reduces harmonics and achieves less heating in induction motors. It has also been compared with classical modulation techniques, and the experimental results show the quality of this PSTM-PWM technique. The modulation technique reduces iron losses due to voltage harmonics and the corresponding magnetic fields that tend to increase core losses, as well as copper losses caused by these harmonics.

The structure of the article is as follows. Section 2 presents an electrical and thermal model for the definition of the heat sources intrinsic to the operation of the induction machine when fed with power inverters. Section 3 presents the peculiarities of the discontinuous modulation technique applied to reduce motor heating. Section 4 shows the assembly that was carried out to feed the motor with H-bridges using the nine-level multilevel converter. Section 5 presents the results of the laboratory implementation. Finally, Section 6 presents the discussion and conclusions.

2. Simplified Thermal–Electrical Modeling of an Induction Machine

In this section, the set of equations governing the losses inherent to operating the machine and the temperatures reached by the stator winding are defined. The most ac-

curate option involves Finite Element Development (FEM), which is most appropriate when the geometry of a machine is to be considered [31]. There are other solutions to identify the thermal issues of the machine and the degree of winding insulation degradation using machine learning models based on genetic algorithms and/or artificial neural networks, which avoid the need for invasive sensors [32]. We have chosen a simplified option for the thermal model: a first-order model for induction motors expressed in Equation (1). This offers multiple advantages and makes it a practical and efficient tool for evaluating heating [33,34].

$$\tau \frac{d\theta(t)}{dt} + \theta(t) = R_{th} \cdot P_{loss}(t) \quad (1)$$

where τ is the thermal time constant (s), $\theta(t)$ is the instantaneous motor temperature (K), R_{th} is the thermal resistance (K/W), and P_{loss} is the loss power (W). In the solution of the equation, the thermal time constant will be

$$\tau = C_{th} \cdot R_{th} \quad (2)$$

By particularizing for an induction machine, specifying the different heat sources, and dividing (1) by R_{th}, Equation (3) is obtained:

$$C_{th} \frac{d\theta(t)}{dt} + \frac{\theta(t)}{R_{th}} = P_{fe}(t) + P_{cu}(t) = P_{loss}(t) \quad (3)$$

$$P_{fe} = k_{fe} \cdot \sum_{h} h^2 \cdot V(h)^2 \quad (4)$$

$$P_{cu} = \sum_{h} R_s(h) \cdot I_s(h)^2 + \sum_{h} R_r(h) \cdot I_r(h)^2 \quad (5)$$

where $\theta(t)$ is the average stator winding temperature, [K]; C_{th} is the equivalent thermal capacity of the machine, [J/K]; R_{th} is the equivalent thermal resistance between the heat source and the environment, [K/W]; P_{cu} is the Joule losses [W]; P_{fe} is the iron losses, [W]; $V(h)$ is the RMS component of the h-harmonic voltage; k_{fe} is the constant determined using no-load tests or the manufacturer's data; $R_r(h)$ is the equivalent rotor resistance at the h-harmonic frequency, which is approximately equal to $R_r \cdot \sqrt{h}$; $R_s(h)$ is the stator resistance at harmonic h and approximately equal to $R_s \cdot \sqrt{h}$; $I_s(h)$ is the RMS component of the harmonic h current in the stator; $R_s(1)$ is the stator resistance at the fundamental frequency; $I_r(h)$ is the current induced in the rotor by harmonic h, which is approximately equal to $k_{tr} \cdot I_s(h)$, where k_{tr} is the rotor–stator transformation coefficient (approximate or calibrated); and $R_r(1)$ is the rotor resistance at the fundamental frequency. The iron losses are complex to calculate as they depend on the magnetic behavior of the hysteresis cycle and the Foucault losses at each electrical harmonic; therefore, the losses were identified via vacuum testing for each of the techniques considered. The losses in the iron will be the losses in the vacuum after subtracting the mechanical losses. Conversely, the losses in copper were calculated with the resistance value of the windings and the harmonic content of the currents.

The technique's mathematical simplicity, based on a single linear differential equation, makes it easy to understand, implement, and solve quickly, without requiring complex simulations. In addition, it requires only a few essential physical parameters, such as thermal resistance and capacitance, which are relatively easy to estimate, thus reducing modeling uncertainty. Although it is a simplified model, it adequately captures the basic heating and cooling dynamics of the motor, including the transient response to changes in losses or load conditions. This feature facilitates its effective integration into real-time thermal monitoring and control systems, helping to prevent overheating damage. Likewise, the first-order

model serves as a basis for more complex and refined developments, maintaining clarity in the thermal analysis. Its low cost, accessibility, and general applicability make it a popular choice for most industries, offering the right balance between accuracy and ease of use for thermal evaluations of induction motors.

In the first-order thermal model used to represent the thermal behavior of an induction motor, the thermal resistance R_{th} plays a key role in relating internal losses to temperature rises. Traditionally, this parameter is considered constant to facilitate analytical calculations; however, under real operating conditions, especially in the presence of harmonics in the power supply, this thermal resistance can be significantly affected, altering the accuracy of the model. As the temperature of the motor increases due to these harmonic losses, the thermal properties of the internal materials begin to change. The thermal conductivity of the insulating materials, copper and steel, decreases with increasing temperatures, reducing the system's ability to transfer heat to the environment. This phenomenon implies an effective increase in R_{th}, although this increase is not evident in static modeling. Additionally, accelerated aging in insulating materials caused by elevated temperatures reduces the overall thermal efficiency of the motor in the long term.

The relationship between winding temperature and Joule losses is a balance between the equations for power that generates heat and the way this heat is transferred to the environment:

$$P_{Joule,\theta} = \sum_{h} I_h^2 R_\theta (1 + \alpha(\theta - 25)) \tag{6}$$

$$P_{conv,\theta} = \pi \cdot \lambda \cdot (\theta_f - \theta_{amb}) \cdot Nu \tag{7}$$

where θ_f is the steady-state temperature, α = 0.003929 [°C^{-1}]; R_θ is the AC resistance of the windings at temperature θ; λ is the thermal conductivity [W/K·m]; and Nu is the Nusselt number. When the motor reaches its thermal steady state, the temperature derivative is zero, and the thermal resistance can be calculated using the following expression:

$$R_{th} = \frac{\theta_f - \theta_{amb}}{P_{loss}} \tag{8}$$

In this work, we analyze how thermal resistance changes as a function of each of the implemented PWM techniques.

The increase in thermal resistance implies that, for the same level of losses, the estimated temperature will be higher, reflecting more critical thermal behavior. If this increase in thermal resistance is not considered in the model, the actual motor temperature may be underestimated, compromising the reliability of the thermal protection system and significantly reducing the life of the motor.

3. Phase Shift Triangle Modulator-PWM Technique

The proposed phase shift triangle modulator (PSTM) method is a pulse-width modulation (PWM) technique that uses a sine wave as a carrier and a triangle wave as a modulator. The triangle wave has a higher peak value than the sine wave, which generates periods of no modulation (no switching), causing overmodulation. To keep the number of switching times constant, the carrier frequency is adjusted according to the peak value of the triangle wave [35]. Thus, the same theoretical modulation index, M, is retained, where $M = f_p/f_m$. Figure 1 shows this technique for M = 15.

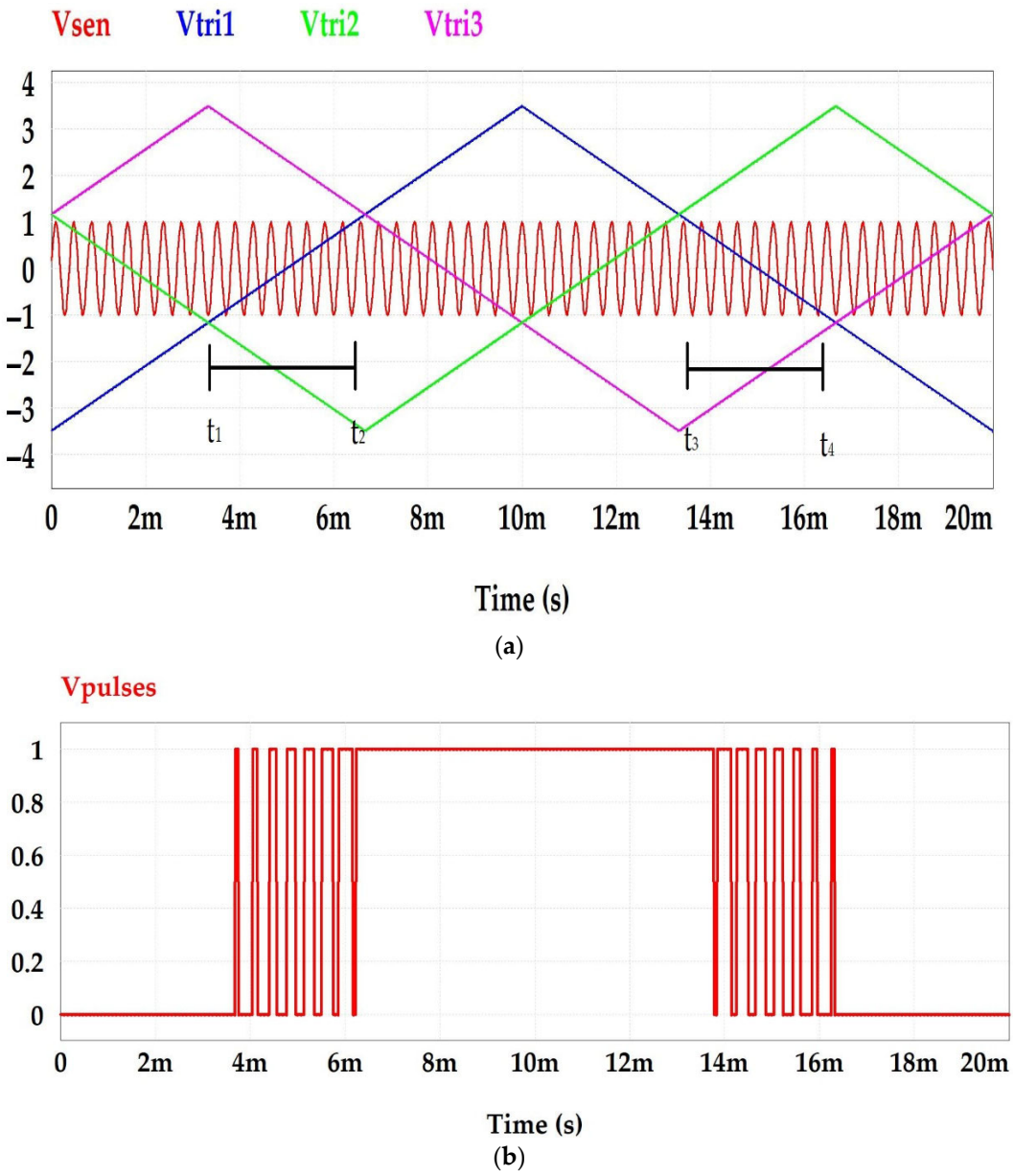

Figure 1. (**a**) Modulating (sine) and carrier (triangular) waves. (**b**) Modulated wave.

To obtain the carrier frequency of the PSTM technique, a sine wave (carrier) is compared with a half-triangular wave (modulator), resulting in a linear equation describing the modulation. From this comparison, the time instants at which the modulation occurs (t_1 and t_2) are calculated:

$$y = -U + \frac{2U}{\pi}\omega_m t \tag{9}$$

$$1 = -U + \frac{2U}{\pi}\omega_m t_b \rightarrow \pi(1+U) = 2U\omega_m t_b \tag{10}$$

$$-1 = -U + \frac{2U}{\pi}\omega_m t_a \rightarrow \pi(U-1) = 2U\omega_m t_a \tag{11}$$

$$1 = -U + \frac{2U}{\pi}\omega_m t_2 = \frac{-U\pi + 2U\omega_m t_2}{\pi} \rightarrow \pi = -U + 2U\omega_m t_2 \tag{12}$$

where U is the peak value of the triangle and ω_m is its pulsation.

$$t_2 = \frac{\pi + U\pi}{2U\omega_m} = \frac{\pi(1+U)}{2U\omega_m} \tag{13}$$

$$t_1 = \frac{U\pi - \pi}{2U\omega_m} = \frac{\pi(U-1)}{2U\omega_m} \tag{14}$$

The period for which the modulation lasts is

$$t = t_2 - t_1 = \frac{\pi + \pi U - \pi U + \pi}{2U\omega_m} = \frac{\pi}{U\omega_m} \tag{15}$$

The carrier frequency can be calculated by knowing how many pulses must be generated in half a period of the modulating signal, i.e., how many pulses are obtained in π radians. The total number of pulses in half a period is

$$x = \frac{\pi M}{2(\omega_m t_2 - \omega_m t_1)} = \frac{\pi M}{2\omega_m(t_2 - t_1)} \tag{16}$$

The number of pulses in a full period of 2π radians will be twice as many:

$$M_t = \frac{\pi M}{\omega_m(t_2 - t_1)} \tag{17}$$

Using Expression (16), the theoretical modulation order is obtained:

$$M_t = \frac{\pi M}{\omega_m \frac{\pi}{U\omega_m}} = UM \tag{18}$$

This indicates that the angular frequency of the carrier is not M (the effective modulation order) because the modulation is discontinuous. It should be UM times that of the modulating signal, which can be considered the modulation order necessary to maintain the number of pulses with respect to a continuous modulation technique:

$$\omega_p = UM\omega_m \rightarrow \ f_p = UMf_m \tag{19}$$

As noted, increasing the number of switches per period generates more heating in the switches and reduces the efficiency of the inverter. Therefore, it is advisable to work with the lowest possible value of M. For the PSTM-PWM technique, a modulation order of $M = 7$ was chosen, complying with EN50160, which sets a maximum THD value of 8%.

4. Experimental Model of the Multilevel H-Bridge Inverter

To determine which peak values of the triangular wave are the most suitable—that is, producing low THD and a high RMS value for the fundamental component—a sweep of U values was performed. The objective was to find the U value that minimizes the THD and maximizes the RMS value of the fundamental, keeping $M = 7$ constant.

Figure 2 shows the THD value as a function of the peak value of the triangular modulator. The maximum value of the sine wave carrier has been kept at 1 V. Minimum THD values are obtained for modulator peak voltages of 1.4 V and 3.5 V.

This technique has been compared with the classical modulation techniques used in H-bridge multilevel inverters: amplitude shift keying (LS-PWM) and phase shift keying (PS-PWM). The results are summarized in Table 1, corresponding to a modulation order of $M = 7$ and a DC supply voltage of $U_c = 100$ V. With these parameters, the proposed technique complies with the requirements established by the EN50160 standard, whereas the classical techniques fail to comply with the regulatory limits due to harmonic values that exceed the allowed maximums.

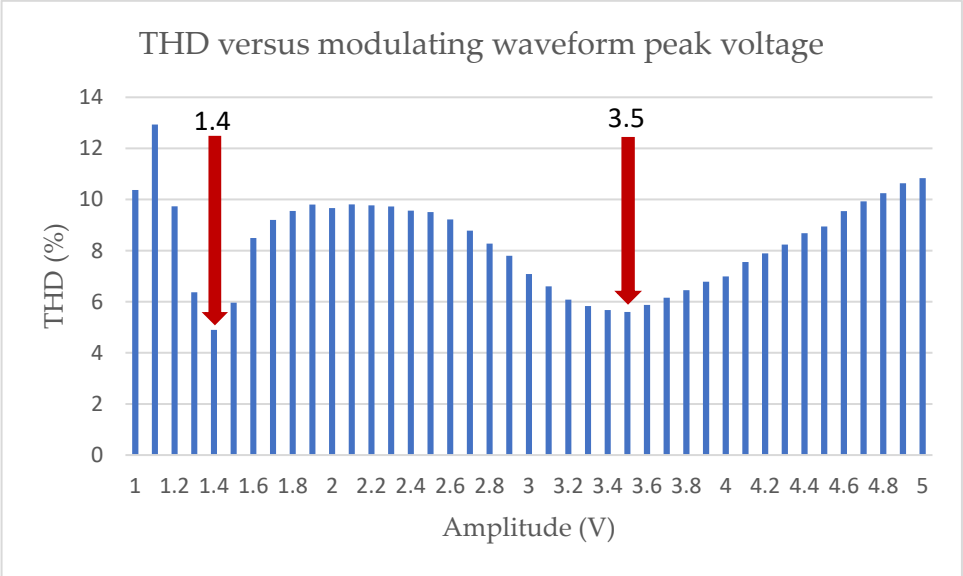

Figure 2. Total harmonic distortion versus triangular modulator amplitude.

Table 1. Harmonic levels (%) of different modulation techniques with multilevel inverter at $M = 7$.

Harm.	Standard EN50160 (%)	LS-PWM (%)	PS-PWM (%)	PSTM-PWM V = 1.4 (%)	PSTM-PWM V = 3.5 (%)
1		100	100	100	100
2	2.000	0.000	0.000	0.005	0.010
3	5.000	3.789	0.193	0.059	0.134
4	1.000	0.000	0.000	0.002	0.004
5	6.000	3.438	0.074	0.819	1.628
6	0.500	0.000	0.000	0.007	0.000
7	5.000	4.195	0.176	4.122	4.001
8	0.500	0.000	0.000	0.006	0.005
9	1.500	3.832	0.037	0.074	0.166
10	0.500	0.000	0.000	0.003	0.004
11	3.500	6.652	0.105	1.656	1.741
12	0.500	0.000	0.000	0.007	0.000
13	3.000	3.677	0.030	0.737	0.782
14	0.500	0.000	0.000	0.006	0.003
15	0.500	1.722	0.051	0.070	0.282
16	0.500	0.000	0.000	0.004	0.003
17	2.000	4.126	0.196	1.347	1.562
18	0.500	0.000	0.000	0.006	0.000
19	1.500	0.160	0.161	0.108	0.337
20	0.500	0.000	0.000	0.008	0.001
21	0.500	4.876	5.017	0.048	0.434

Table 1. *Cont.*

Harm.	Standard EN50160 (%)	LS-PWM (%)	PS-PWM (%)	PSTM-PWM V = 1.4 (%)	PSTM-PWM V = 3.5 (%)
22	0.500	0.000	0.000	0.009	0.002
23	1.500	1.715	11.772	1.007	1.290
24	0.500	0.000	0.000	0.008	0.000
25	1.500	4.761	0.090	0.412	0.627
Fund. Value RMS		250.51	243.95	221.32	295.57
THD25 (%)	8	13.62	12.83	4.89	5.59

Notably, none of the classical techniques manage to comply with the level of THD required by the standard for a modulation order of $M = 7$.

An AEG motor with the following parameters was used to validate the proposed technique: AEG three-phase induction motor—rated voltage: 220 V/380 V; rated power: 0.3 kW; rated current: 1.65 A; frequency: 50 Hz; rated speed: 1450 rpm; rated slip: 0.05626; power factor: 0.829; number of poles: four; rated efficiency: 81.56%; rated torque: 6.82 Nm; starting current: 5.5 times rated; starting torque: 2.7 times nominal; maximum torque: 2.8 times nominal.

To implement the multilevel inverters, the GPT-IGBT module from (GUASCH S.A™, Barcelona, Spain) was utilized. This module constructs an H-bridge using insulated gate bipolar transistors (IGBTs) for motor control applications. It incorporates a three-phase bridge rectifier, a capacitor bank, IGBTs with a forced air-cooled heat sink, opto-isolated drivers, output phase current sensors, a DC-Link current sensor, and a DC-Link voltage sensor. The main electrical specifications include a maximum DC-Link voltage of 750 V and a maximum current output per phase of 32 A.

To generate the control signals for the inverter stages, hardware from National Instruments was employed, specifically, the NI9154™ module. A LabVIEW™ (2020 version, Austin TX, EEUU)-based platform was developed to implement various PWM techniques. Voltage harmonics at the inverter output were measured using three-phase power analyzers, while power quality was assessed with the Chauvin Arnoux™ C.A 8336 (Asnières-Sur-Seine, France), which can measure up to the 50th harmonic. The DC supply voltage (Uc) feeding the H-bridges was set to 100 V. The experimental laboratory setup is illustrated in Figure 3.

Figure 4 shows oscillograms of the classical PWM techniques: LS-PWM (Figure 4a) and PS-PWM (Figure 4b). Figure 5 shows oscillograms of the proposed PWM technique for two V values: PSTM-PWM, V = 1.4 (Figure 5a), and PSTM-PWM, V = 3.5 (Figure 5b).

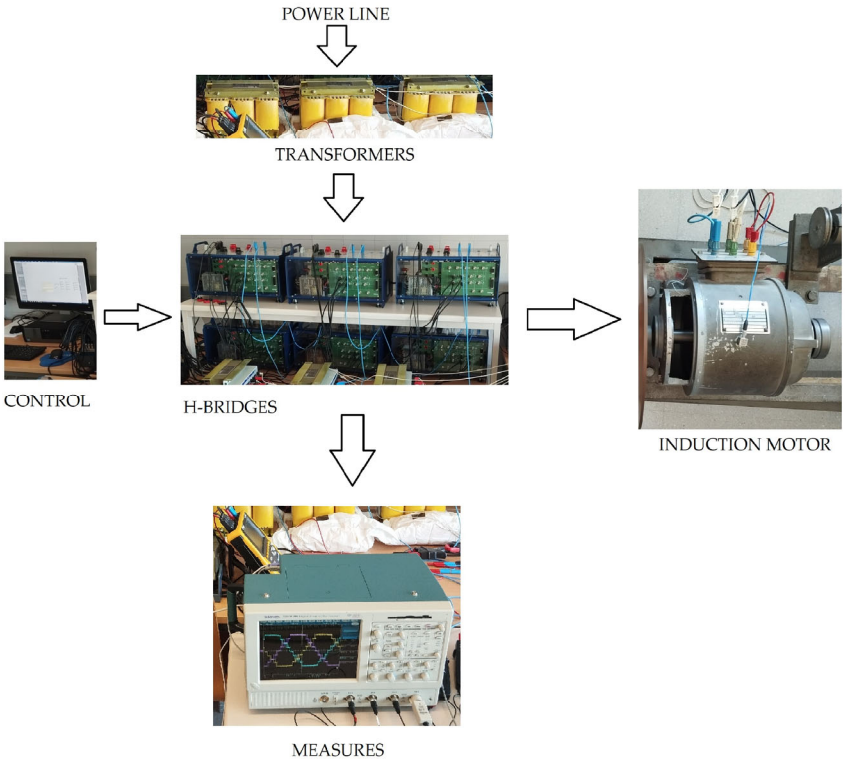

Figure 3. Experimental laboratory setup: control, H-bridge, measurements, and motor.

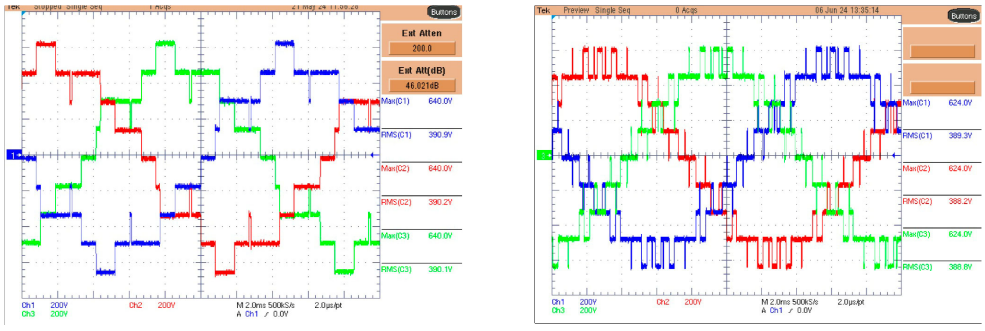

(**a**) (**b**)

Figure 4. Oscillograms of PWM techniques: (**a**) LS-PWM; (**b**) PS-PWM.

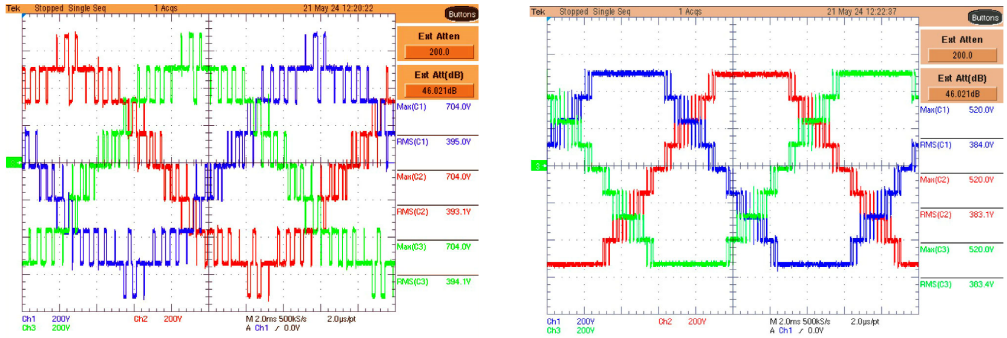

(**a**) (**b**)

Figure 5. Oscillograms of PWM techniques: (**a**) PSTM-PWM, U = 1.4; (**b**) PSTM-PWM, U = 3.5.

5. Experimental Results

To select the measurement location, the motor was pre-warmed for 30 min. The hottest points were observed with a thermographic camera, and the points of the coil that were the

hottest were chosen, with one located between the coil passage slot and the coil itself and the other in the curved part of the coil under the insulator, in addition to the thermocouple that measures the internal ambient temperature (Figure 6a). Figure 6b details the position of the thermocouple on the stator coil head.

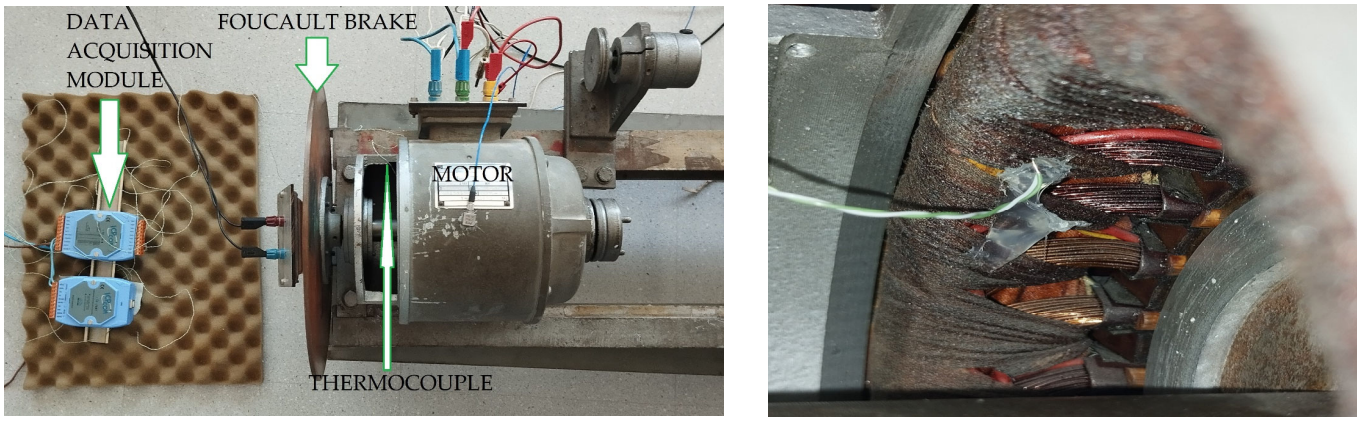

(**a**) (**b**)

Figure 6. (**a**) Data acquisition module for thermocouples and Foucault brake connected to the motor. (**b**) Detail of the position of the thermocouple that measures the head temperature of the stator coil.

The motor was supplied with a voltage of 380 V RMS for fundamental harmonic in-star mounting in all techniques. The load consisted of an eddy-current-fed brake to adjust the power consumed to 300 W (nominal power rating). The total power consumed by the machine was also measured to evaluate the power losses of each technique. A controlled ambient temperature of 25 °C was assumed for all techniques.

For an accurate evaluation of heating in an induction motor, it is essential to measure the temperature directly in the stator windings. This can be achieved via integrated temperature sensors such as thermocouples, which provide accurate readings of the motor's internal temperature.

Notably, the accuracy of thermocouples can range from ±0.5 °C to ±2.0 °C, depending on factors such as the type, the quality of the mounting, and the calibration of the acquisition system.

During the process, care was taken to keep the experimental conditions constant: the sensor was stably fixed to ensure good thermal contact, and a uniform acquisition frequency was maintained for all measurements. These precautions minimized systematic errors associated with variations in positioning or reading times. To evaluate the consistency and stability of the measurements under controlled conditions, 15 consecutive measurements were taken at the same sampling point.

Based on the data, the basic statistical parameters were calculated: the arithmetic mean as a representative value of the measured temperature and the standard deviation as an estimate of the dispersion of the readings. Under stable conditions and with good mounting, the standard deviation was consistent with what is expected for this type of sensor, located in a range of approximately ±0.3 °C to ±0.6 °C. These values reflect both the sensitivity of the sensor and small local thermal variations in the system under study.

The temperature on the outside of the motor and windings was also measured using a thermographic camera. Notably, measuring the temperature on the external surface of the motor does not accurately indicate the internal temperature of the windings, as the casing can be significantly cooler than the inside of the motor.

To evaluate losses, vacuum and short-circuit tests were carried out. The vacuum test was used to determine the iron and mechanical losses. The latter were evaluated

by representing the vacuum losses as a function of the quadratic power supply voltage, obtaining these mechanical losses on the ordinate axis, with a value of 19.45 W. The copper losses were calculated with the value of the short-circuit test resistance, R_{cc} (stator resistance, R_s, and rotor resistance from the stator, R_r), with a value of 20.1 Ω, together with the harmonic currents of each technique implemented (Figure 7). Note that the fundamental term of the current is truncated to 0.4 A to provide greater clarity to the harmonic terms. Based on the tests, thermal resistance was calculated for each technique using Equation (8). Table 2 below shows the average values of the 15 temperature measurements made and, therefore, the calculated values of these thermal resistances.

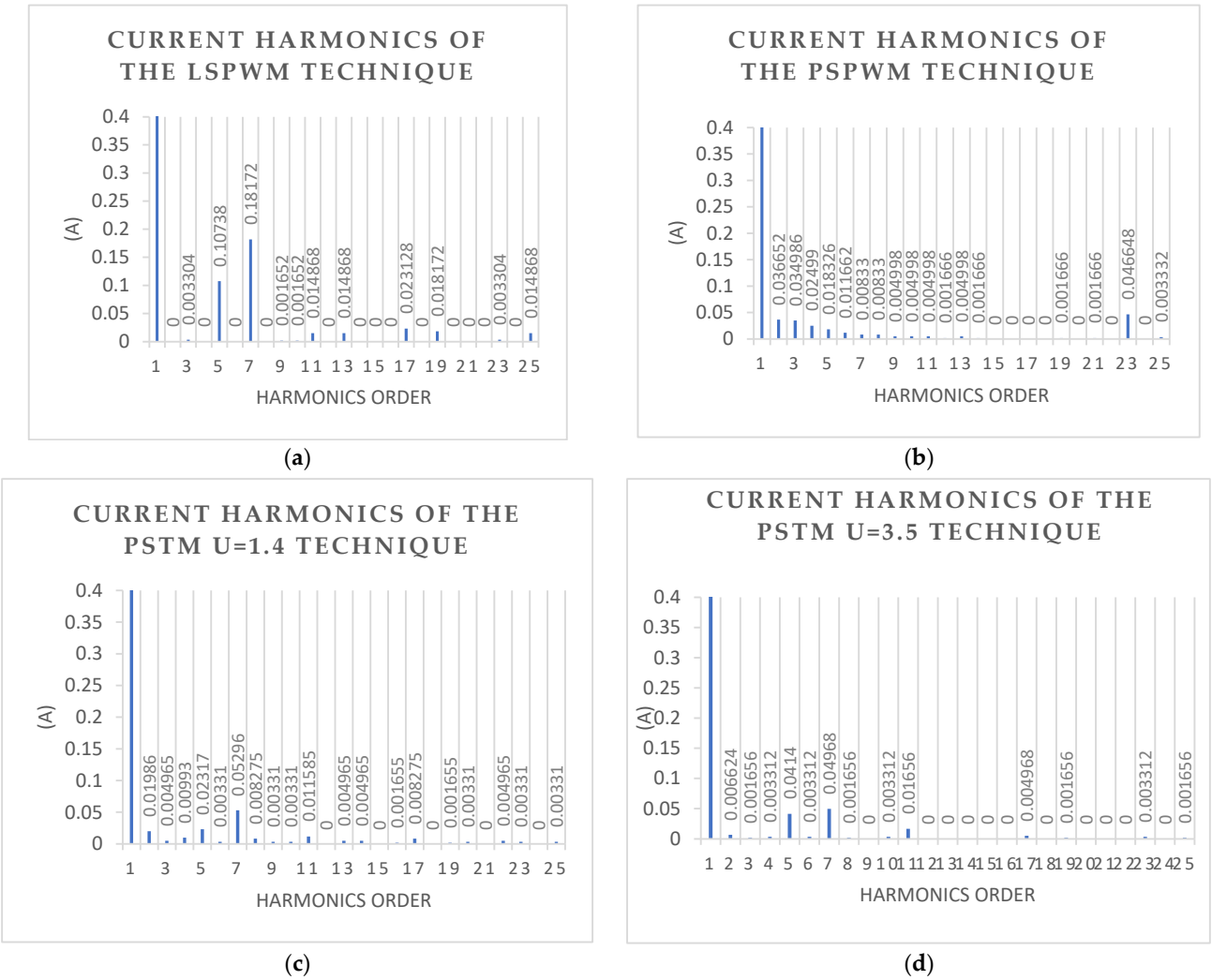

Figure 7. RMS amplitude harmonic currents: (**a**) LSPWM; (**b**) PSPWM; (**c**) PSTM, U = 1.4; and (**d**) PSTM, U = 3.5.

Table 2. Thermocouple temperature, losses, and thermal resistance for different techniques.

	Temperature (°C)	P_{fe} (W)	P_{cu} (W)	R_{th} (K/W)
LSPWM	63.2	30.58	54.91	0.446
PSPWM	61.1	29.11	53.94	0.434
PSTM U = 1.4	60.3	27.95	53.62	0.432
PSTM U = 3.5	59.5	27.46	52.41	0.426

With the proposed technique, losses are reduced due to the lower harmonic content.

The following figures show images obtained with the thermographic camera for the techniques tested. There is a difference between the temperatures provided with the measurements made with the thermocouples and those provided with the thermographic camera, as the thermographic camera measures areas and not specific points; thus, it can have errors of $\pm$ 1 degree. Thermocouple readings are more accurate. However, during the test, there is a correlation between the techniques used and the measurements, both with the thermographic camera and the thermocouples. Of the measurements made, those corresponding to the thermocouples are taken as valid. Figure 8 shows images of the motor measurements taken with the techniques created using the thermographic camera: (a) LS-PWM, (b) PS-PWM, (c) PSTM-PWM U = 1.4, and (d) PSTM-PWM U = 3.5.

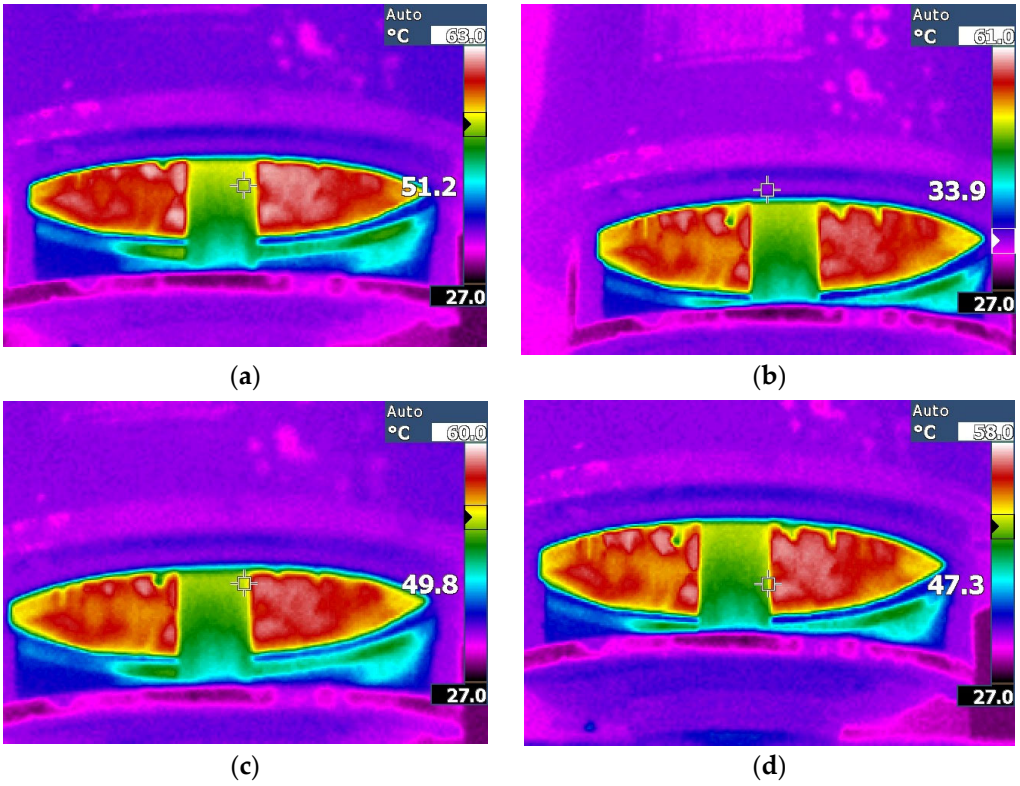

Figure 8. Thermographic images of the techniques: (**a**) LSPWM; (**b**) PSPWM; (**c**) PSTM, U = 1.4; and (**d**) PSTM, U = 3.5.

6. Discussion and Conclusions

This study shows that harmonics generated by power inverters have a significant impact on the thermal behavior of induction motors, increasing their internal losses—mainly due to the Joule effect—and, to a lesser degree, iron losses and phenomena such as the pellicular effect. These additional losses increase the temperature of the stator windings, the most thermally sensitive element, which compromises the lifespan of the insulation and thus the reliability and durability of the motor. To measure such an increase, an easy access point is the stator winding heads. Thus, the thermocouples were placed at this location.

To mitigate these effects, a new PSTM-PWM (pulse-width phase shift triangle modulation) technique was implemented and experimentally evaluated, applied to an H-bridge type multilevel inverter. This technique is distinguished by the use of a sinusoidal signal as carrier and a triangular signal with overmodulation as modulator, effectively reducing the harmonic content of the inverter output signal. The modulation order parameter was

kept constant at $M = 7$ to keep the number of switching operations as low as possible and to comply with the requirements of the EN50160 standard, as opposed to conventional techniques that do not comply with it. It is true that this is not mandatory, but it is recommended. In addition, to minimize power inverter losses and reduce the generation of high-voltage pulses with steep voltage transitions (high dV/dt)—which can lead to the long-term degradation of the insulation in induction motor windings—the modulation order was set to $M = 7$.

During laboratory tests, three modulation techniques were compared: LS-PWM, PS-PWM, and two configurations of the proposed PSTM-PWM technique (with peak values of $U = 1.4$ V and $U = 3.5$ V for the triangular signal). To ensure homogeneous conditions, the AEG motor used was subjected to a constant load of 300 W using a Foucault brake, with a supply voltage of 380 V RMS corresponding to the fundamental harmonic. Temperatures were measured at the winding heads using thermocouples and a thermographic camera.

The results indicate that the PSTM-PWM technique—especially with U equal to 3.5 V—significantly reduced the internal temperature of the motor compared with the classical techniques. The average temperature recorded in the winding was 59.5 °C with this technique, compared with 63.2 °C obtained with LS-PWM, representing a clear reduction in thermal stress. In addition, total lower internal losses were observed (80.87 W for PSTM-PWM versus 85.49 W for LS-PWM). Thermal resistance was determined experimentally at the high-temperature point that could be accessed. Given the difficulty of determining this accurately (as FEM modeling would allow for), we opted to compare different modulation techniques to determine the temperature differences under the same load conditions. Future work could include the application of the technique to other power topologies, to different types of motors, and the estimation of temperature using neural networks or genetic algorithms.

In summary, the experimental results confirm that the PSTM-PWM technique not only meets the regulatory requirements in terms of total harmonic distortion (THD) but also enables a remarkable improvement in the thermal behavior of induction motors fed by multilevel inverters. This implies a reduction in motor heating, reduced insulation aging, higher energy efficiency, and a possible extension of the equipment's lifespan. Therefore, the PSTM-PWM technique constitutes an effective and practical technical alternative to conventional modulation strategies, especially in industrial applications where power quality and thermal reliability are critical factors.

Author Contributions: A.R.-G., conceptualization and methodology; F.M.P.-H., J.-R.H.-L. and M.M.-G., simulation and data collection; A.R.-G., F.M.P.-H., J.-R.H.-L. and M.M.-G., hardware implementation; A.R.-G., writing—original draft preparation; A.R.-G., F.M.P.-H., J.-R.H.-L. and M.M.-G., validation and writing—review and editing; F.M.P.-H., funding acquisition. All authors have read and agreed to the published version of the manuscript.

Funding: This research received no external funding.

Data Availability Statement: The data are contained in this study.

Acknowledgments: During the preparation of this manuscript/study, the authors used ChatGPT to improve the English text. The authors have reviewed and edited the output and take full responsibility for the content of this publication.

Conflicts of Interest: The authors declare no conflict of interest.

References

1. Tabora, J.M.; Tostes, M.E.d.L.; de Matos, E.O.; Soares, T.M.; Bezerra, U.H. Voltage harmonic impacts on electric motors: A comparison between IE2, IE3 and IE4 induction motor classes. *Energies* **2020**, *13*, 3333. [CrossRef]
2. NEMA MG 1—"Motors and Generators" National Electrical Manufacturers Association 1300 North 17th Street, Suite 1752, Rosslyn, VA 22209, USA. Available online: https://www.weg.net (accessed on 10 June 2025).
3. Umesh, H.; Rashmi, K. Causes and Effect of Inverter Harmonics. In *Current Perspective to Physical Science Research 6*; Dong, S.-H., Ed.; BP International: Ciudad de Mexico, Mexico, 2024; pp. 70–89. [CrossRef]
4. Beleiu, H.G.; Maier, V.; Pavel, S.G.; Birou, I.; Pică, C.S.; Dărab, P.C. Harmonics consequences on drive systems with induction motor. *Appl. Sci.* **2020**, *10*, 1528. [CrossRef]
5. Gnaciński, P.; Pepliński, M.; Muc, A.; Hallmann, D.; Klimczak, P. Induction motors under voltage fluctuations and power quality standards. *IEEE Trans. Energy Convers.* **2023**, *39*, 1255–1264. [CrossRef]
6. Fuchs Ewald, F. Are harmonic recommendations according to IEEE-519 and CEI/IEC 555 too restrictive? In Proceedings of the Frontiers of Power Conference, Stillwater, OK, USA, 4 October 2002; Engineering Energy Laboratory, Oklahoma State University: Stillwater, OK, USA, 2002; pp. 1–18. Available online: https://www.researchgate.net/publication/290494727 (accessed on 5 August 2025).
7. Mirza, A.Y.; Bazzi, A.; Nguyen, H.H.; Cao, Y. Motor stator insulation stress due to multilevel inverter voltage output levels and power quality. *Energies* **2022**, *15*, 4091. [CrossRef]
8. Saeed, M.; Fernández, D.; Guerrero, J.M.; Díaz, I.; Briz, F. Insulation Condition Assessment in Inverter-Fed Motors Using the High-Frequency Common Mode Current: A Case Study. *Energies* **2024**, *17*, 470. [CrossRef]
9. Debruyne, C.; Vandevelde, L.; Desmet, J. Harmonic Effects on Induction and Line Start Permanent Magnet Machines. Available online: https://www.researchgate.net/publication/264195127 (accessed on 5 August 2025).
10. Fatima, A.; Kumar, R.; Li, Z.; Byczynski, G.; Kar, N.C. Modelling of Inductances Considering Bar Harmonics and Temperature to Accurately Predict Output Torque of an Induction Motor. *IEEE Access* **2024**, *12*, 156561–156571. [CrossRef]
11. Abramov, B.I.; Datskovskii, L.K.; Kuz'min, I.K.; Shevyrev, Y.V. Electric drives of mining installations. *Russ. Electr. Eng.* **2017**, *88*, 159–165. [CrossRef]
12. Donolo, P.; Bossio, G.; De Angelo, C.; García, G.; Donolo, M. Voltage unbalance and harmonic distortion effects on induction motor power, torque and vibrations. *Electr. Power Syst. Res.* **2016**, *140*, 866–873. [CrossRef]
13. De abreu, J.P.G.; Emanuel, A.E. Induction motor thermal aging caused by voltage distortion and imbalance: Loss of useful life and its estimated cost. In Proceedings of the 2001 IEEE Industrial and Commercial Power Systems Technical Conference, New Orleans, LO, USA, 13–17 May 2001; Conference Record (Cat. No. 01CH37226). IEEE: New York, NY, USA, 2001; pp. 105–114. [CrossRef]
14. Husach, S. Python-based Induction Motors Monitoring and Lifetime Estimation System. In Proceedings of the IEEE International Conference on Modern Electrical and Energy Systems (MEES), Kremenchuk, Ukraine, 21–24 September 2021; IEEE: New York, NY, USA, 2021; pp. 1–4. [CrossRef]
15. Rusu-Zagar, C.; Notingher, P.; Navrapescu, V.; Mares, G.; Rusu-Zagar, G.; Setnescu, T.; Setnescu, R. Method for estimating the lifetime of electric motors insulation. In Proceedings of the 2013 8th International Symposium on Advanced Topics in Electrical Engineering (ATEE), Bucharest, Romania, 23–25 May 2013; IEEE: New York, NY, USA, 2013; pp. 1–6. [CrossRef]
16. Muxiri, A.C.P.; Bento, F.; Fonseca, D.S.B.; Cardoso, A.J.M. Thermal analysis of an induction motor subjected to inter-turn short-circuit failures in the stator windings. In Proceedings of the 2019 International Conference on Industrial Engineering, Applications and Manufacturing (ICIEAM), Sochi, Russia, 25–29 March 2019; IEEE: New York, NY, USA, 2019; pp. 1–5. [CrossRef]
17. Singh, G.K. A research survey of induction motor operation with non-sinusoidal supply wave forms. *Electr. Power Syst. Res.* **2005**, *75*, 200–213. [CrossRef]
18. Khelfi, H.; Hamdani, S.; Hamouda, S.; Baghdouche, K.K.; Ammari, Z.; Attab, A. Analysis of Harmonic and Noise Influence on Temporal Envelope Estimation for Detecting Broken Rotor Bars in Asynchronous Machines. In Proceedings of the 2nd International Conference on Electrical Engineering and Automatic Control (ICEEAC), Setif, Algeria, 12–14 May 2024; pp. 1–6. [CrossRef]
19. Zhu, W.; De Gaetano, D.; Chen, X.; Jewell, G.W.; Hu, Y. A review of modeling and mitigation techniques for bearing currents in electrical machines with variable-frequency drives. *IEEE Access* **2022**, *10*, 125279–125297. [CrossRef]
20. *DIN EN50160*; Voltage Characteristics of Electricity Supplied by Public Distribution Networks. DIN: German Institute for Standardization: Berlin, Germany, 2025.
21. Dugan, R.C.; McGranaghan, M.F.; Santoso, S.; Beaty, H.W. *Electrical Power Systems Quality*, 2nd ed.; McGraw Hill Companies: New York, NY, USA, 2004.
22. Rata, G.; Rata, M.; Graur, I.; Milici, D.L. Induction Motor Speed Estimator Using Rotor Slot Harmonics. *Adv. Electr. Comput. Eng.* **2009**, *9*, 70–73. [CrossRef]

23. Beleiu, H.G.; Miron, A.; Pavel, S.G.; Cziker, A.C.; Niste, D.F.; Darab, P.C. Impact of Voltage Unbalance and Harmonics on Induction Motor Efficiency. In Proceedings of the IEEE International Conference and Exposition on Electric and Power Engineering (EPEi), Iasi, Romania, 17–19 October 2024; pp. 328–332. [CrossRef]
24. Dargahi, V.; Abarzadeh, M.; Corzine, K.A.; Enslin, J.H.; Sadigh, A.K.; Rodriguez, J.; Blaabjerg, F.; Maqsood, A. Fundamental Circuit Topology of Duo-Active-Neutral-Point-Clamped and Duo-Neutral-Point-Piloted Multilevel Converters. *IEEE J. Emerg. Sel. Top. Power Electron.* **2019**, *7*, 1224–1242. [CrossRef]
25. Rodriguez, J.; Bernet, S.; Steimer, P.K.; Lizama, I.E. A survey on neutral-point-clamped inverters. *IEEE Trans. Ind. Electron.* **2010**, *57*, 2219–2230. [CrossRef]
26. Hasegawa, I.; Kondo, T.; Kodama, T. Experiment of five-level BTB-system with common flying capacitors. In Proceedings of the 8th IET International Conference on Power Electronics, Machines, and Drives, PEMD, Glasgow, UK, 19–21 April 2016.
27. Malinowski, M.; Gopakumar, K.; Rodriguez, J.; Perez, M.A. A survey on cascaded multilevel inverters. *IEEE Trans. Ind. Electron.* **2010**, *57*, 2197–2206. [CrossRef]
28. Leon, J.I.; Vazquez, S.; Franquelo, L.G. Multilevel converters: Control and modulation techniques for their operation and industrial applications. *Proc. IEEE* **2017**, *105*, 2066–2081. [CrossRef]
29. Aslam, A.W.; Hassan, J.; Minambres-Marcos, V.; Al-Salloomee, A.G.S.; Roncero-Clemente, C. Traditional and Hybrid Topologies for Single-Three-Phase Transformerless Multilevel Inverters. *Electronics* **2024**, *13*, 4058. [CrossRef]
30. Choudhury, S.; Bajaj, M.; Dash, T.; Kamel, S.; Jurado, F. Multilevel Inverter: A Survey on Classical and Advanced Topologies, Control Schemes, Applications to Power System and Future Prospects. *Energies* **2021**, *14*, 5773. [CrossRef]
31. Wu, W.; He, Y.; Ma, J.; Lu, Q.; Qiu, L.; Fang, Y. Temperature Analysis of Secondary Plate of Linear Induction Motor on Maglev Train Under Periodic Running Condition and Its Optimization. *Machines* **2025**, *13*, 495. [CrossRef]
32. Szamel, L.; Oloo, J. Monitoring of Stator Winding Insulation Degradation through Estimation of Stator Winding Temperature and Leakage Current. *Machines* **2024**, *12*, 220. [CrossRef]
33. Nogal, Ł.; Magdziarz, A.; Rasolomampionona, D.D.; Łukaszewski, P.; Sapuła, Ł.; Szreder, R. The laboratory analysis of the thermal processes occurring in low-voltage asynchronous electric motors. *Energies* **2021**, *14*, 2056. [CrossRef]
34. Moreno, J.F.; Hidalgo, F.P.; Martinez, M.D. Realization of tests to determine the parameters of the thermal model of induction machine. *Proc. IEE Electr. Power Appl.* **2001**, *148*, 393–397. [CrossRef]
35. Heredia-Larrubia, J.-R.; Perez-Hidalgo, F.M.; Ruiz-Gonzalez, A.; Meco-Gutierrez, M.J. Discontinuous Multilevel Pulse Width Modulation Technique for Grid Voltage Quality Improvement and Inverter Loss Reduction in Photovoltaic Systems. *Electronics* **2025**, *14*, 2695. [CrossRef]